Reconfigurable responsive structures assembled from magnetic Janus particles†‡

Stoyan K. Smoukov,[a] Sumit Gangwal,[a] Manuel Marquez[bc] and Orlin D. Velev*[a]

Received 18th August 2008, Accepted 27th November 2008
First published as an Advance Article on the web 26th January 2009
DOI: 10.1039/b814304h

Magnetic Janus particles are assembled into novel staggered chain structures under the action of magnetic and electric fields. The magnetic assembly can result in permanent structures, which could be disassembled on demand by remote demagnetization.

Introduction

Responsive materials are used in many diverse applications including actuators, sensors, tunable viscosity liquids, and displays. In addition to materials with controlled properties, a number of "smart" building blocks are promising as components of responsive assemblies. Electro-[1,2] and magneto-rheological[3] fluids rely on such assemblies for their dynamic change in viscosity. The design of building blocks with novel and directional interactions has resulted in nanoparticle superlattice crystals based on light-induced dipole-switching,[4] and colloid assemblies by AC electric field-induced polarization.[5,6]

The response of a material or structure is usually coupled to a change in the environment (temperature, pH, applied field) and when such a change occurs naturally, responsive structures can be used to detect it. In many cases, however, an environmental change is maintained solely to keep a structure/material in a given state, which wastes energy or requires good insulation from the surroundings. Some conditions required to sustain a certain structural response (*e.g.*, electric fields of 1–2 kV/mm for electrorheological fluids[7,8]) are also impractical to maintain for long periods of time.

A solution to this problem can be found in bistable (or multistable) systems where the states of interest can occupy local potential energy minima, with high activation barriers between them prohibiting interconversion. Such macroscopic switches and latches are explored in energy-efficient robotics designs.[9] Microscopically, such designs are found in MEMS actuators[10] and optical switches.[11] Miniaturization also requires one to take advantage of forces that dominate on the micron scale and below (magnetic, electrostatic, van der Waals), resulting in different device designs and opportunities. When bistability is engineered at the level of the building blocks, the whole structure formed by the blocks can assemble and disassemble in a bistable fashion.

Ferromagnetic interactions are particularly suitable for assembly of multistable structures because ferromagnetic moments do not require external fields to be maintained and magnetization strength can be varied easily. A variety of well-characterized magnetic materials can be easily evaporated or sputter-deposited with a sub-nanometer-level precision. Well-defined structures assembled from magnetic colloids reported in the literature include linear chains,[12–16] zigzag chains,[17] magnetic nanowires,[18] 2D arrays,[19] static and dynamic lattices on the surface of fluids,[20,21] pyramids,[22] and rings.[23,24] Magnetic field-assembled structures have important applications – magneto-rheological fluids owe many of their properties to formation of linear chains and their crystallization in clusters due to lateral interactions of the dipolar chains.[25] Magnetic assembly has also been used in microfluidic mixers utilizing the rotation of self-assembled paramagnetic and ferromagnetic chains,[26,27] in solutions with magneto-optical responses, which can cover the whole visible range,[17,28] and in hierarchical assembly of particles.[29] Magnetic beads connected with polymer linkages have resulted in flexible, responsive brush structures on surfaces.[30] Polymers loaded with magnetic particles have a number of applications including magnetically actuated cilia.[31] Non-magnetic polymer rods have been ordered by magnetic fields when placed in the bulk of a ferrofluid.[32]

Substantial interest in polarization-induced chaining of particles exists because of electro- and magneto-rheological fluids, where linear chains and multichain aggregates form upon application of an electric or magnetic field, dynamically changing the fluid's viscosity by several orders of magnitude. Applications of these fluids include clutches with no moving parts,[33] vibration-reduction,[34] and semi-active control dampers for seismic protection of buildings.[35] Well-defined, non-linear structure assembly from polarizable building blocks is still rare, however, and is likely hampered by the complexity of modeling the interactions.

The polarization induced in particles at low applied electric and magnetic fields is directly proportional to the field magnitude; at large distances, the interaction U_{ij}^{dip} between two dipoles is proportional to the square of the applied field and inversely proportional to the third power of the distance between them.[36] For particles near contact, mutual polarization can increase their interaction by more than an order of magnitude,[37] so addition of multipole interactions or finite element calculations are necessary to approximate the experimental results.[38,39] High electric fields

[a]*Chemical and Biomolecular Engineering Dept., NC State University, Raleigh, NC, 27695, USA. E-mail: odvelev@ncsu.edu*
[b]*Harrington Dept. of Bioengineering, Arizona State University, Tempe, AZ, 85287, USA*
[c]*NIST Center for Theoretical and Computational Nanosciences, Gaithersburg, MD, 20899, USA*

† This paper is part of a *Soft Matter* theme issue on Self-Assembly. Guest editor: Bartosz Grzybowski.

‡ Electronic supplementary information (ESI) available: Movies 1–3 and Supplementary Fig. 1 and 2. See DOI: 10.1039/b814304h

This journal is © The Royal Society of Chemistry 2009

near the tips of contacting particles can cause the dispersing medium to break down, leading to a current-controlled interaction and changing $U_{ij}^{dip} \propto E^2$ to $U_{ij}^{dip} \propto E^{1.2}$.[40] Higher magnetic fields cause ferromagnetic materials to saturate, requiring one to measure their field dependent magnetization and apply micromagnetic models to predict their interactions.

Here we report on the reconfigurable assembly of structures composed of Janus particles – polystyrene spheres with a thin magnetic metal shell evaporated on one hemisphere. The anisotropic particles assemble in low symmetry structures, which are well-defined and are stable in the absence of applied fields or supplied energy. The structures also have the advantage that the particle interactions are bistable. They can be disassembled on demand by remote demagnetization, then reassembled into new stable structures, thus recycling the building blocks.

Experimental

Materials

Polystyrene latex microspheres (diameter $D = 4.0$ μm) with amine or sulfate surface groups were purchased as surfactant-free aqueous dispersions from Interfacial Dynamics Corp. (Eugene, OR). Non-ionic surfactant polyoxyethylene(20) sorbitan monolaureate (Tween® 20, CAS# [9005-64-5]) was purchased from Acros Organics (Morris Plains, NJ). Ethanol and Teflon tape were purchased from Fisher Scientific. Iron (99.95% pure) pellets and gold (99.99% pure) wire were purchased from Kurt J. Lesker Co. (Clairton, PA). Chromium-plated tungsten rods were purchased from R. D. Mathis Co. (Long Beach, CA). Deionized water with a resistivity of 18.2 MΩ cm was obtained from a Millipore Milli-Q Plus water purification system.

Preparation of magnetic Janus particles

The magnetic Janus particles were prepared by partially coating one hemisphere of the polystyrene microspheres with an 8 or 34 nm layer of iron (Fig. 1A). The polystyrene particles were initially concentrated by centrifuging at ~1500 *g* for 5 minutes and were then washed with ultra-pure Milli-Q water. This step was repeated 2–3 times to remove any surfactants or electrolytes present in the media. A convective assembly method that was previously developed in our laboratory[41] was used to deposit particle submonolayers on pre-cleaned glass microscope slides (Fisher Scientific). Deposition of particle submonolayers was preferred because we did not want the presence of multilayers, which may occur when forming close-packed particle monolayers[41] and could result in uncoated particles. The dried particle submonolayers were coated with 8 or 34 nm of iron (Fe) on the exposed top hemisphere in a metal evaporator (Cooke Vacuum Products, model FPS2-41). The thickness of the evaporated iron layer was monitored by a Maxtek, Inc. TM350 thickness monitor integrated in our metal evaporator, with SC-101 sensor crystals. No adhesion layer was used. The particles were then scraped gently from the deposition surface with the corner of a microscope slide, and re-suspended in an ultra-pure Milli-Q water solution of a non-ionic surfactant Tween-20 (~1 wt%). The role of the surfactant was to prevent nonspecific particle aggregation. The typical volumes used in each experiment were 2–5 μL, resulting in suspensions with ~90 000–150 000 particles/μL or ~0.3–0.5% solids.

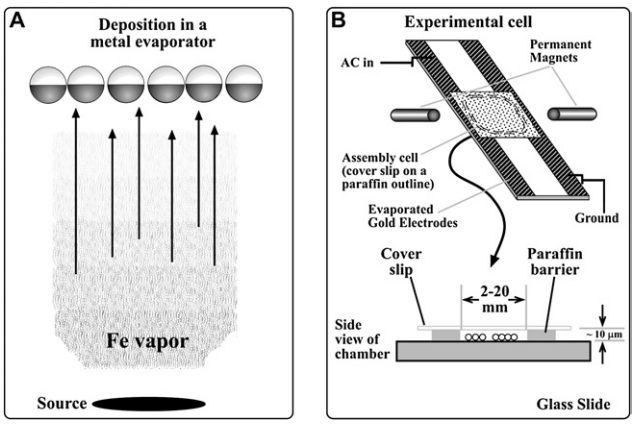

Fig. 1 (A) Schematic of Janus particle fabrication by evaporation of a magnetic coating onto a monolayer of latex colloid spheres on a substrate. (B) Experimental cell used to apply electric and magnetic fields.

Experimental setup

An experimental cell constructed above a glass slide (Fig. 1B) was used to apply magnetic and electric fields to the Janus microspheres. A 2–5 μL particle droplet suspension was placed in the middle of the cell in a hydrophobic ring "corral", which was deposited by a liquid blocker pen. A microscope glass cover slip was placed on top of the particle-containing droplet, causing the droplet to spread to the edge of the hydrophobic ring. The cell thickness was approximately 2–3 particle diameters. Permanent magnets were situated near the sides of the glass slide to apply magnetic fields. Two co-planar gold electrodes (3 mm inter-electrode gap) were deposited by metal evaporation (with 10 nm of chromium followed by 100 nm of gold) on the sides of the glass slide to allow the application of electric fields.

Particle chaining in the experimental cell was observed from above using an Olympus BX-61 optical microscope (50× objective). Images were recorded using an Olympus DP-70 digital CCD camera. Time-lapse movies with frame delays of 2–10 s were taken with this camera using the DP Controller microscope software. Real-time digital movies of the magnetic Janus particles' response to applied electric and magnetic fields were recorded using a Sony Cybershot DSC-V1 camera fitted to the eyepiece of the microscope.

The constant magnetic field was created by a pair of cylindrical permanent magnets (Magcraft, NSN0537/N40, $d = 6.4$ mm, $l = 19.2$ mm, $B_R = 12.9$ kG, $H_C = 11.9$ kOe). The magnets were aligned on a single axis on each side of the observation cell, the south pole of one facing the north pole of the other, with a 20 mm distance between them. The magnetic flux density at the point of observation (near the magnet axis, midway between the magnets) was estimated at 0.15 T from the manufacturer's specifications and finite element modeling of the field. Magnetization measurements were performed on an alternating gradient magnetometer (AGM) – MicroMag model 2090, Princeton Measurement Corporation. A NIST magnetic moment standard (a YFe garnet sphere with 76.67 emu – standard reference

 This journal is © The Royal Society of Chemistry 2009

material #2853) was used for calibration. Samples were attached to the probe with Dow Corning silicone grease #112.

For AC electric field assembly, an alternating electric field was applied to the electrodes of the observation cell. The square waveform (with frequencies of 1–400 kHz) was produced by an Agilent 33120A 15 MHz function generator (Agilent Technologies, CO). The function generator was connected to a RG-91 ramp generator/amplifier (Burleigh, NY) to produce voltages ranging from 1–90 V. The electric circuit included a 1 μF capacitor to remove any direct current component of the signal. The voltage applied in the chamber was measured with a multimeter GDM8024 (Good Will Instrument Co, Taiwan), which readings were correlated to measurements with an oscilloscope. A master switch connected to the two co-planar gold electrodes of the experimental cell allowed the electric field to be turned on and off.

Demagnetization of chains of magnetic Janus particles was performed by applying a 60 Hz alternating magnetic field to the assemblies using a Tenma CRT Demagnetization Coil (MCM Electronics, Centerville, OH, item #72-785). For demagnetization of samples with Fe layers >30 nm, a homemade coil with a field directed by an E-shaped transformer core was used. The samples were placed in the center of the demagnetizing coil for a few seconds and slowly moved away from it (10–15 s). Thus, the magnitude of the magnetic field at the sample was decreased continuously as the distance from the coil was increased, while its direction switched at 60 Hz. This allowed the magnetic sample to trace ever smaller magnetization hysteresis loops[42] until it was demagnetized.

Numerical simulation

Two-dimensional (2D) magnetostatic calculations were performed using the FEMLAB multiphysics modeling package (COMSOL, Burlington, MA) to obtain the magnetic field distribution and magnetic energy distribution around the Janus particles. The geometry of the system, to scale, was specified as a 2D cross-sectional top view at the midpoint of the experimental cell in Fig. 1B. The particle configurations were arranged vertically rather than horizontally in the simulations. The magnetic and electric field directions were also from top to bottom of the simulation. The magnetic Janus particles (simulated with 4 μm diameter) were positioned midway between the applied magnets.

The solution space was divided into three subdomains: water media, dielectric polystyrene core, and a thin 34 nm iron (Fe) layer on one-half of the particle. To reproduce the tapering of the coating towards the sides of the particle, the coating profile was modeled by the subtraction of two circles with diameters equal to those of the particle spheres and centers offset by the thickness of the metal coating (see details in Supplementary Fig. 1).

The physical property values for electrical conductivity (σ) and relative permeability (μ) for each of these subdomains were specified as: water media ($\sigma = 1 \times 10^{-4}$ S/m, $\mu = 1 - \chi_m = 1 - 9.04 \times 10^{-6}$), polystyrene core ($\sigma = 1 \times 10^{-16}$ S/m, $\mu = 1 - \chi_m = 1 - 8.21 \times 10^{-6}$), and iron layer ($\sigma = 1 \times 10^{+7}$ S/m, $\mu = 7.00$) where χ_m is the magnetic susceptibility. We specified in the simulation a homogeneous applied magnetic field of 0.15 T (123 400 A/m) from the top to the bottom side of the box with an electric insulation boundary condition on the sides. We placed 8 particles in different configurations inside the box and initiated the FEMLAB simulation. The solution space was then triangulated into a conformal mesh and the mesh was refined. The program was initialized to solve the Maxwell equations for all elements to obtain the magnetic field intensity and magnetic energy density within the cell. The magnetic energy of the entire 2D configuration was calculated using the subdomain integration function. This tool integrated the magnetic energy density over the area (since this was a 2D simulation) of the system, after selecting all three of the subdomains. The calculations were repeated with more refined mesh sizes until the mesh was small enough for the final calculated values to vary by less than 0.05%. In most simulations the mesh was refined approximately three times.

To convert to a 3D energy calculation (with effective units of J), we multiplied the 2D simulation energy by the radius of the particle, modeling the particle as a cylinder. While the 2D simulation captures the right trends and distinguishes magnetic energies between various multi-particle configurations (with effective units of J/m), we expect that this methodology overestimates the absolute interaction values near the inter-particle contact area.

3. Experimental results

The originally dispersed Janus particles were assembled into various chain structures using single or combined magnetic and/

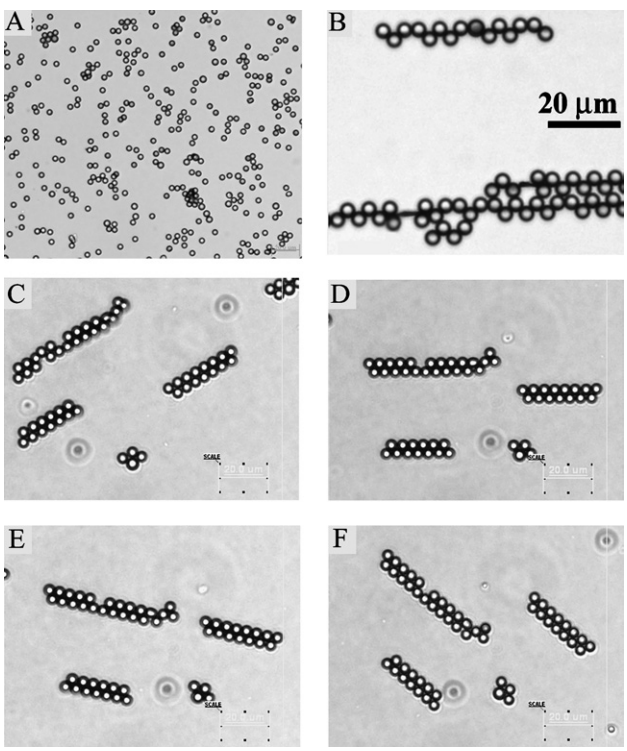

Fig. 2 Micrographs of assemblies of Janus particles with 8 nm evaporated Fe layer on the surface. (A) Before the application of magnetic fields. (B) "Staggered" and (C) "Double" chains that form in a magnetic field of ~0.15 T. Both types of chains in (B) and (C) orient with the magnetic field, and rotate around their center of mass. Rotation of a staggered chain is shown in Supplementary Movies 1 and 2. (C)–(F) illustrate the rotation of an ensemble double chains.

or AC electric fields. The initial suspensions before applying magnetic fields contained disordered particles, including some clusters (Fig. 2A). Upon application of a magnetic field (~0.15 T) the particles assemble quickly into chains of various structure (Fig. 2B,C), reconfiguring the clusters to form chains. Whether the initial aggregation is due to small initial magnetization of the iron coating on the particles, or to adhesion forces resulting from the bridging of neighboring particles with nanometer-sized metal layers, those forces are typically much weaker than the magnetic field-induced ordering producing the chains. The chains oriented along the field direction and, upon rotation of the field, reoriented to match the direction as can be seen in Supplementary Movies 1 and 2. Two types of structures were observed – a "staggered chain", illustrated in Fig. 2B, and the "double chain" structure in Fig. 2C. The particles in the staggered chain align with their metal halves touching the metal halves of adjacent particles, which face in alternating directions. The metal parts of the particles thus form a metal lane in the middle of the chain, but their polystyrene sides stick out and do not touch other particles on the same side of the chain axis. Occasionally, two adjacent particles are trapped facing on the same side of a staggered chain (Fig. 2B, Fig. 3C). The double chain structure consists of two single chains of particles with metal parts facing the same way, which pair up to form a double chain. In both structures the touching metal parts form a path in the middle of the chain, and both structures seem to be metastable states of the particle assembly. The "double" chain structure was only observed for particles with 7–8 nm Fe layers, while the staggered chain structure was observed for particles with higher magnetic moments (thicker evaporated magnetic layers). In select cases, the staggered chains were observed for 7–8 nm layer particles at higher applied fields, but the application of such fields was not uniform and hard to characterize. Computational simulations are under way to calculate the magnetic energies stored in each structure and any field-dependent energy barriers between them. Preliminary results suggest that either structure could be a stable configuration, depending on the metal layer thickness.

The staggered chains not only orient with the direction of the applied field, but are also strong enough to withstand drag forces. Intact chains, as the ones pictured in Fig. 2C–2F, are observed for rotation speeds up to 60 rpm. When two chains come close enough, they can connect to form a single long chain which continues to orient with the field, rotating around its new center of mass (see Movie 2 of the ESI‡).

Upon application of AC electric fields, the freely dispersed particles (Fig. 3A) polarize (as in Fig. 4A) and assemble into chain structures (Fig. 3B). These chains are more close-packed, compared to the previously observed "staggered chains" assembled from gold/polystyrene metallodielectric microspheres in AC electric fields.[43] They often form first as single chains and consequently stick together in pairs. Presumably, the lower conductivity and polarizability of an 8 nm iron layer, compared

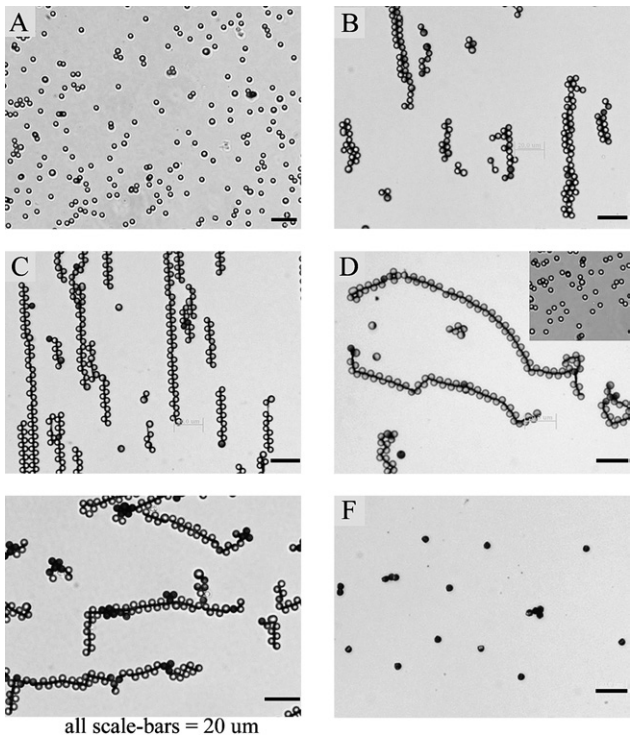

Fig. 3 Optical micrographs of: (A) Particles in the absence of field; (B) Particles assembled using AC electric fields (400 kHz, 25 V peak-to-peak); (C) Particle assemblies in a magnetic field of ~ 0.15 T. (D) The particles remain in chains after removal of the magnetic field. (D-inset) chains of particles with 8 nm Fe layer broken up by tapping on the experimental cell. (E) Particles with 34 nm Fe layer would not fall apart with tapping on the experimental cell, though (F) they disassemble after demagnetization with an AC coil. All scale bars = 20 μm.

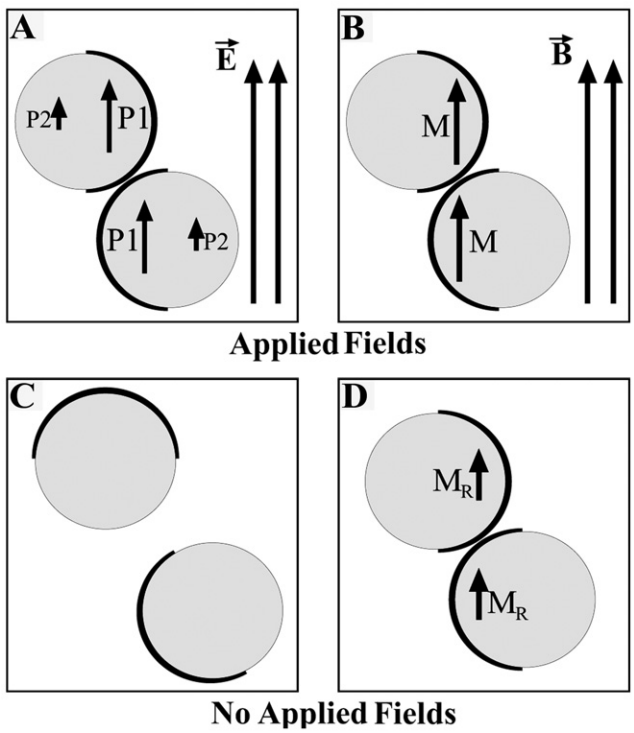

Fig. 4 Modes of the interaction of magnetic, metallodielectric Janus particles in: (A) electric field; (B) magnetic field. (C) Following system (A), after removal of the electric field. (D) Following system (B) after removal of the magnetic field. The dark thin arc-shaped shell represents the gold coating (for applied electric fields) or iron coating (for applied magnetic fields) on one hemisphere of the polystyrene core particles.

This journal is © The Royal Society of Chemistry 2009

with those of a 20 nm gold layer, may be a reason for the double and single chain formation, which is observed in the limit of pure polystyrene spheres in AC electric fields.[44,45]

Fig. 3 also illustrates one of the main differences observed for the assembly of such half-shell particles in magnetic *vs.* electric fields. When magnetic fields were applied, the staggered chain (Fig. 2B, 3C) and the double chain (Fig. 2C) structures were observed. These chains remain assembled even after the removal of the magnetic field (Fig. 3D), though they curve due to local field effects. When the concentration of particles was high, even upon removal of the directing magnetic field, the chains largely kept their orientation due to lack of room to reconfigure (see Supplementary Fig. 2). The formation of permanent chains is due to the remnant magnetization in the metal shells, and is unlike that of chains assembled in electric fields (Fig. 3B), which simply fall apart upon removal of the AC electric fields. The magnetic chains (formed at lower surface concentration of particles) can be switched between curved and straight configurations by repeated application and removal of the field. They can also be disassembled by demagnetization (Fig. 3F) and completely reconfigured into new chains by subsequent application of a magnetic field.

Another distinguishing feature of magnetic field interactions is that they are not screened in solution, as opposed to the exponential screening of electrical interactions due to counterions. This makes magnetic interactions both much stronger and easier to predict at ranges >100 nm. (For a monovalent ion concentration range of 10 μM to 1 mM, the Debye length at which an electrical charge is largely screened is ~100 nm and 10 nm, respectively. By contrast, magnetic interactions are almost independent of the content of the usual aqueous solutions.) The electrically assembled particles quickly and spontaneously disassemble in the absence of a field due to the action of Brownian motion. By contrast, the magnetized particles have residual magnetization and form stable assemblies, which are hard to break. The forces between the Janus particles can be tuned by changing the thickness and type of magnetic material shell evaporated on them. Chains from Janus particles covered with 8 nm Fe layer fall apart easily due to shear forces from light tapping on the observation cell (Fig. 3D – inset). By contrast, chains of particles with a 34 nm Fe layer do not fall apart (Fig. 3E) and need to be demagnetized in order to be disassembled (Fig. 3F).

The physical origins of the assembly processes based on polarization in electric and magnetic fields are shown schematically in Fig. 4. Note that in electric fields, both the metal shell (dark thin coating) and the polystyrene core polarize, and contribute to the interaction, though the dipole on the polystyrene side is smaller (Fig. 4A). By contrast, for magnetic fields the properties of polystyrene or water media are similar to those of vacuum and their contribution is negligible (Fig. 4B). Upon removal of the field, the electrically assembled particles disassemble, whereas the magnetic particles remain polarized and assembled (Fig. 4C,D).

The assembly of particles in chains due to a magnetic field is found usually to result in the "staggered chain" configuration, observed previously for metallodielectric spheres under applied AC electric fields.[43] The dipolar interactions of magnetized and electrically polarized Janus particles are similar in physical origin, though there are also significant differences. In the case of AC electric fields, the major force behind the polarization and the interaction of the spheres are ionic flows in the counterionic atmospheres of the particles. Even at contact, while the polarization of the metal parts of a sphere largely determines the assembly configuration, polarization and counterionic flows on the polystyrene side are still significant. In the case of magnetic fields, the permeabilities of water and polystyrene are so close to those of vacuum that, except for steric packing considerations, it is possible to ignore them and consider the magnetic interactions only among the metal half-shells.

Another difference between clustering of chains in AC electric fields[43] and between the magnetic chains is revealed in the dynamics of their lateral interactions. When magnetic chains approach each other they do not come together laterally to crystallize, as observed with electric field assembly.[44] The magnetic chains instead move away from each other toward each others' ends and join end-to-end to form a longer chain. This indicates a slight long-range lateral repulsion between the chains.

Measurements of the saturation and residual magnetization of the particles allow us to estimate the magnetization parameters used in our model for particles in a chain at a given field, and to estimate the strength of the particle–particle interactions in the absence of a magnetic field. The magnetization hysteresis loops for magnetic Janus particles with 8 and 34 nm coatings of Fe, as well as for flat thin layers of Fe of the same thicknesses, are shown in Fig. 5. The saturation magnetization for the thin films is lower than that of bulk iron (1707 emu/cm^3)[46] (Table 1). The results are consistent with literature reports.[47] Flat thin films also show directional anisotropy, with magnetization in the perpendicular direction much smaller than in the plane of the film (Fig. 5C,D). For 8 nm Fe films the difference is almost one hundredfold. When a film is on the surface of a polystyrene sphere, given its curvature, parts of the film are always at an angle to the applied field, resulting in lower total magnetization. This is consistent with the lower magnetization of films on particle surfaces compared to the parallel magnetization of flat 2D films of the same thickness. We found that these differences in directional magnetization explain differences in particle assembly observed with changing the magnetic coating thickness.

To understand why individual magnetic Janus particles orient with the plane between their iron-capped and polystyrene hemispheres parallel to the direction of the magnetic field and to model the formation of chain configurations, we calculated the magnetic energy of the system for different orientations of a single particle and for chain configurations of several particles. We performed 2D FEMLAB simulations of the magnetic field distribution and energy density of the Janus particle–media system. The favorable configurations minimize the potential energy of the particles, and also maximize the magnetic energy stored in the system.

The magnetic energy stored in the system is directly related to the magnetic field intensity in the cell. The local magnetic energy density w_B for particles in vacuum is: $w_B = \frac{1}{2}\frac{B^2}{\mu_0}$ where B is the magnetic field intensity, and μ_0 is the permeability of free space ($4\pi \times 10^{-7}\ N/A^2$).[48] The total magnetic energy W_B of the system can be obtained by integrating w_B over the subdomain volume (V): $W_B = \int_V w_B \, \mathrm{d}V$.

We found that the shape of the coating profile is important for predicting packing configurations, and even for obtaining the

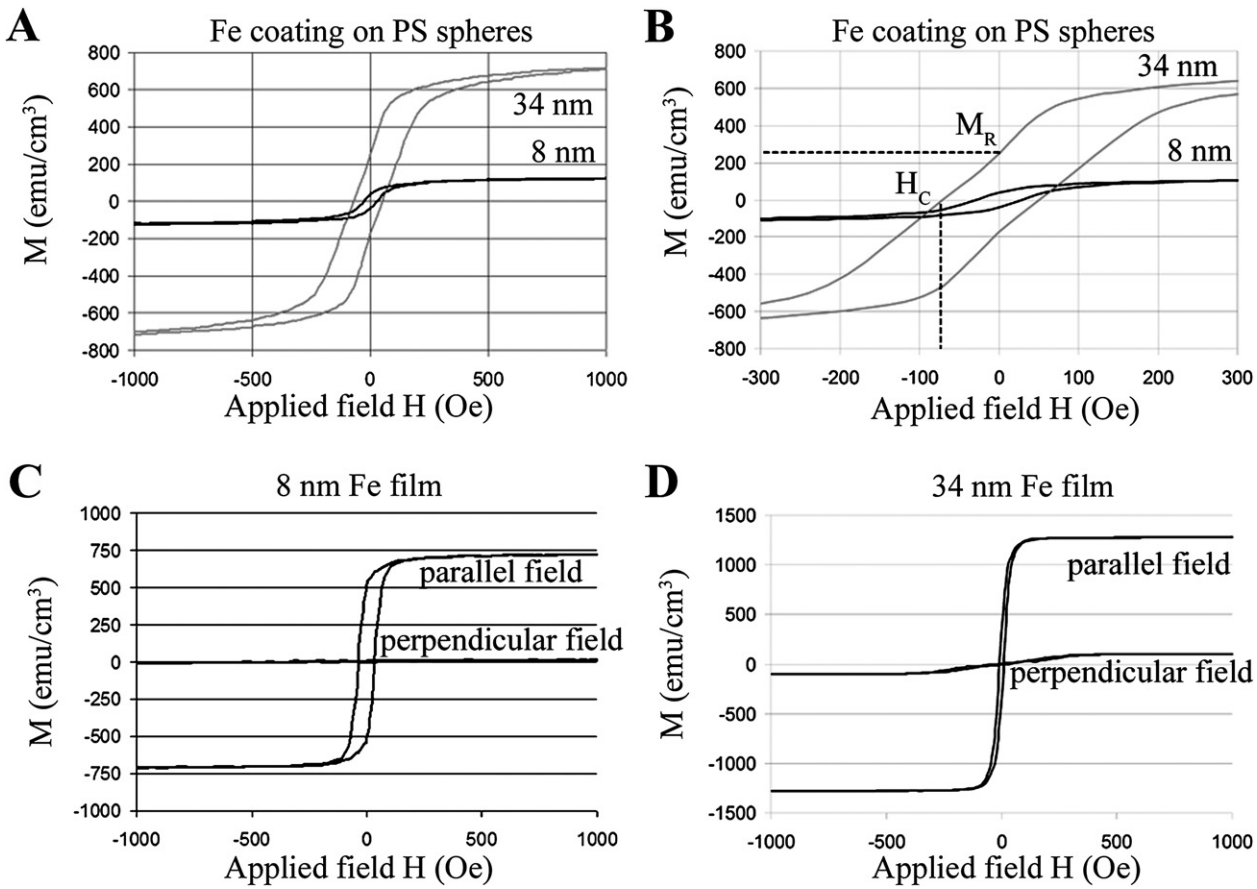

Fig. 5 **(A)** Magnetization hysteresis curves for 8 nm and 34 nm Fe coatings on PS spheres. **(B)** Zoom of (A) near zero field shows the residual magnetization (M_R) and coercive fields H_C) for the samples. **(C)** Magnetization of a flat 8 nm Fe film in the direction parallel and perpendicular to the film. Virtually no magnetization is observed perpendicular to the film. **(D)** Magnetization of a flat 34 nm Fe film in the direction parallel and perpendicular to the film.

Table 1 Summary of the measured and estimated magnetic parameters

Material	M_S (emu/cm^3)	M_R (emu/cm^3)	H_C (Oe)
Particles			
8 nm film on PS spheres	125 ± 25	30 ± 10	25
34 nm film on PS spheres	740 ± 60	285 ± 15	80
Films			
8 nm flat film – parallel H	750 ± 30	525 ± 30	35
8 nm flat film – perpendicular H	12	6	205
34 nm flat film – parallel H	1280 ± 40	350 ± 10	10
34 nm flat film – perpendicular H	105	8	33

energy of a single sphere oriented in the field. As the atomic evaporation flux is projected onto the curved surface of the spheres, the coatings are thickest in the center facing the evaporation source, and taper out to zero at the sides where the evaporation flux is tangential to the sphere surface (illustrated in Supplementary Fig. 1).

Simulations of a single Janus magnetic sphere demonstrate that its lowest potential energy orientation occurs when the plane between its iron-capped and bare polystyrene hemispheres is parallel to the direction of the applied magnetic field (Fig. 6A-inset). The potential energy difference between the -90° orientation angle (where the plane is aligned perpendicular to the magnetic field direction) and the 0° orientation was estimated to be $\sim 10^6 kT$ under the actual experimental conditions ($B = 0.15$ T and $\mu = 7.00$ of the 34-nm-thick iron coating, as listed in the experimental section). For comparison, the potential energy difference in an applied AC electric field of 10 kHz, 100 V/cm was $\sim 100 kT$ for the same orientation angles.[43] The difference in calculated potential energy between the $-90°$ and 0° orientation angles decreases significantly when a thinner iron layer (having lower permeability) is used in the simulations. The differences between electric and magnetic interactions are even more apparent in the absence of applied fields. Induced electrical polarizations disappear and the chains disassemble due to Brownian motion, whereas remnant magnetic interactions keep the chains intact due to the 34-nm iron-coating residual magnetization of 285 000 A/m (obtained from the magnetization hysteresis curve in Fig. 5A).

The preferred orientation of an individual iron-coated Janus particle in a magnetic field is the same as the gold-coated Janus particles in an electric field. When assembled in a field, the particles formed staggered chain where the metal coatings face the chain center line and touch those of neighboring particles (Fig. 6A), while the bare polystyrene halves face in alternating directions along the chain. For staggered-chain particle assemblies the alternating arrangement makes it possible to specify

 This journal is © The Royal Society of Chemistry 2009

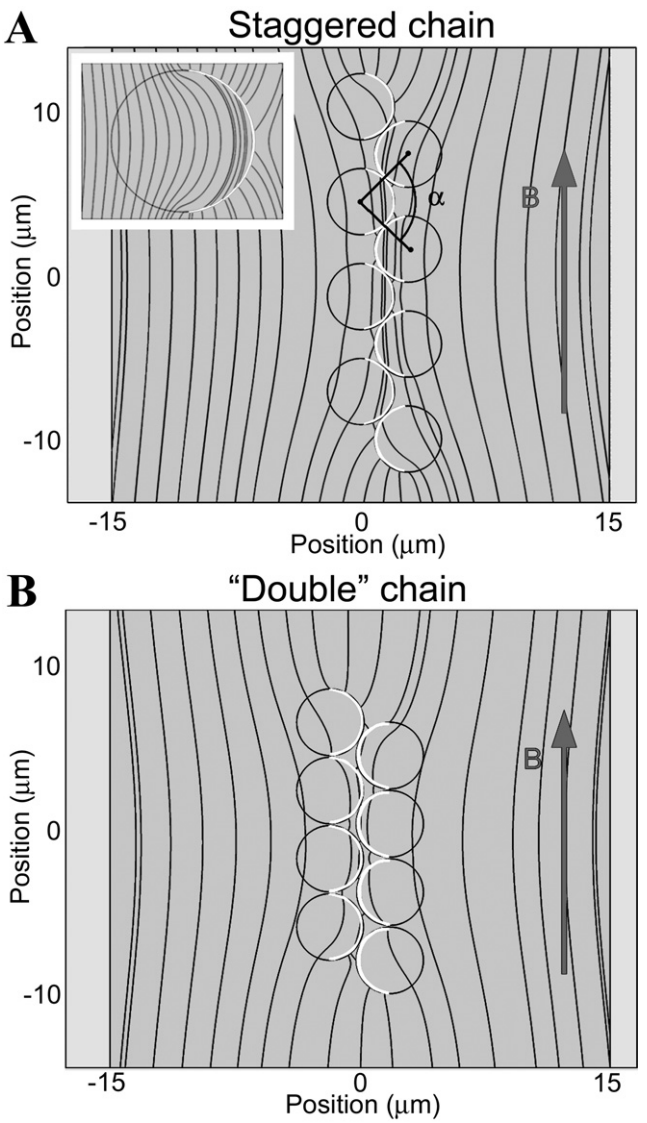

Fig. 6 Simulations of the magnetic energy density contours in an applied magnetic field around different magnetic Janus particle configurations: (A) Eight-particle staggered chain; (A – inset) Single particle with iron coating (on right side of particle) aligned in the direction of magnetic field; (B) Eight-particle double chain. The streamlines indicate the direction of the magnetic field and the density of the streamlines is proportional to the magnitude of the field. The pale-coloured arcs represent the iron shell in (A) and (B). The simulations were performed at a low magnetic field strength (100 A/m), so that a higher permeability value of 520 (read from the magnetization hysteresis curve in Fig. 5A) in the iron coating could be used, which allowed the magnetic field streamlines around the particles to be easily distinguished.

a chain configuration by specifying the angle between any three adjacent particles (designated α in Fig. 6A) We performed "quasi-Monte Carlo" simulations[43] of configurations of eight particles by varying this angle (in increments of 20 degrees) and calculating the total stored magnetic energy until we found the configuration with the maximum stored magnetic energy. The simulations show the lowest potential energy arrangement to be the one in Fig. 6A, with $\alpha = 90$ degrees. This result matches well the configuration angle observed in experiments (89 ± 5 degrees) for particles with Fe metal coatings thicker than 21 nm.

The "double chain", two linear chains stuck together with the iron shells facing inside (or a close-packed staggered chain with $\alpha = 60$ degrees, Fig. 6B) was found to be unfavorable by $\sim 28\,000\,kT$ per particle compared to $\alpha = 90$ degrees (Fig. 6A). More detailed simulations are under way to explain the experimental configuration. Most likely, the reason is the anisotropic magnetization of the iron layers of different thickness (Fig. 5 C,D) where thin layers show virtually no susceptibility in the perpendicular direction. Since the sides of the particles are covered with thinner metal layers, and their curvature places them perpendicular to the applied field, large parts of the side coating of the particles are not magnetized. For thin layers exhibiting orders of magnitude difference in susceptibility between the two orientations, the "double" chain configuration might become favorable.

Discussion

The data demonstrate that magnetic interactions could provide strong, yet reversible, binding of structural assembly blocks even in the absence of applied fields. They also provide convenience and simplicity in engineered assembly. Most common media, including aqueous solvents and dielectrics, have a magnetic permittivity very close to that of vacuum, so the prediction and design of interparticle interactions is relatively straightforward. Magnetic interactions are not screened in solution allowing action at large distances, unlike electrostatic interactions, which decrease exponentially, even at nanometer distances. Supplementary Movie 3 illustrates the movement of a particle along a gradient of an applied magnetic field. It approaches a cluster of other particles, changes trajectory substantially due to the local magnetic field from the cluster and finally sticks to it. The effect is seen 6–7 particle diameters away from the cluster whereas, by comparison, electric fields show such an effect only 1–2 particle diameters from a cluster, and even then probably due to hydrodynamic rather than electrostatic interactions. For this reason we observe much faster consolidation of individual magnetic particles into clusters than of AC electric field-driven metallodielectrics.

One of the advantages of electric fields is that they are much easier to apply in devices, by simple conductor wires, which potentially decreases the device size and complexity. Changing the direction of magnetic fields requires the use of multiple magnetic coils or, alternatively, moving parts with permanent magnets. Electric fields also can be applied at a wider range of operating frequencies, which are not limited by the inductance of a magnetic coil.

Anisotropic magnetic particles enable the assembly of complex lattices in external fields. The interactions between the components are tunable by the choice of magnetic material, amount deposited, as well as by partial magnetization. It is clear that the local magnetic fields around our particles play a significant role in producing the curved chain structures (Fig. 3D,E) in the absence of the external magnetic field. Micromagnetic simulations are currently under way in our lab in order to elucidate the particles' behavior away from the strong field limit. As pointed out in Fig. 5C,D, the thin layers in our Janus particles exhibit directional magnetic anisotropy and their curvature produces complex magnetization patterns as

a function of the external field. Literature reports document the possibility of field-induced symmetry breaking[49,50] or a change in the preferred magnetization direction[51] in particles. One potential outcome of understanding such behavior in detail is the creation of a structure from identical particles, which can be reconfigured into different well-defined equilibrium structures just by changing the strength of the applied field.

Potential applications of the linear assemblies include reconfigurable microwires and circuits if the metal contacts formed during assembly are conductive. Chemical modifications of the polystyrene and metal surfaces of the particles could make possible reagent binding and detection and lead to microwire sensors.

Functional structures with metastable states, based on magnetic interactions similar to the ones studied here, could be created and disassembled on command. This ability will bring them closer to the new "cradle-to-cradle" design of building block reuse, much like the full recycling of components in natural life cycles. Challenges on the road include manufacturing of novel and versatile building blocks with directional binding, leading to even more complex structure assemblies.

In conclusion, we have demonstrated not only self-assembly of novel magnetic structures, but also their rapid on-demand disassembly by remote demagnetization. Our method provides a route to the reversible structures and the reuse and recycling of the particle building blocks. Fine-tuning of the particle interactions is possible by sub-nanometer control of evaporated magnetic domains, or by partial magnetization.

Acknowledgements

This study was supported by a NIRT project from the National Science Foundation (CBET 0506701) and a visiting researcher fellowship from the Interdisciplinary Network for Emerging Science and Technologies. We thank Mr. Oliver Luen for his help in performing the magnetization measurements.

References

1 A. P. Gast and C. F. Zukoski, *Adv. Colloid Interface Sci.*, 1989, **30**, 153–202.
2 T. Hao, *Adv. Colloid Interface Sci.*, 2002, **97**, 1–35.
3 J. Liu, M. Lawrence, A. Wu, M. L. Ivey, G. A. Flores, K. Javier, J. Bibette and J. Richard, *Phys. Rev. Lett.*, 1995, **74**, 2828–2831.
4 R. Klajn, K. J. M. Bishop and B. A. Grzybowski, *Proc. Natl. Acad. Sci. USA*, 2007, **104**, 10305–10309.
5 S. Gangwal, O. J. Cayre, M. Z. Bazant and O. D. Velev, *Phys. Rev. Lett.*, 2008, **1**, 058302.
6 O. D. Velev and K. H. Bhatt, *Soft Matter*, 2006, **2**, 738–750.
7 R. T. Bonnecaze and J. F. Brady, *J. Rheol.*, 1992, **36**, 73–115.
8 L. C. Davis, *J. Appl. Phys.*, 1992, **72**, 1334–1340.
9 M. Hafez, M. D. Lichter and S. Dubowski, *Trans. Mechatr.*, 2003, **8**, 18–25.
10 J. Qiu, J. H. Lang and A. H. Slocum, *J. Microelectromech. Syst.*, 2004, **13**, 137–146.
11 C. Lee and C. Y. Wu, *J. Micromech. Microeng.*, 2005, **15**, 11–19.
12 F. Caruso, A. S. Susha, M. Giersig and H. Mohwald, *Adv. Mater.*, 1999, **11**, 950–953.
13 S. Melle and J. E. Martin, *J. Chem. Phys.*, 2003, **118**, 9875–9881.
14 F. M. Pedrero, M. T. Miranda, A. Schmitt and J. C. Fernandez, *J. Chem. Phys.*, 2006, **125**, 084706.
15 S. Melle, O. G. Calderon, M. A. Rubio and G. G. Fuller, *Int. J. Mod. Phys. B*, 2002, **16**, 2293–2299.
16 J. Lin, W. L. Zhou, A. Kumbhar, J. Wiemann, J. Y. Fang, E. E. Carpenter and C. J. O'Connor, *J. Solid State Chem.*, 2001, **159**, 26–31.
17 J. P. Ge, Y. X. Hu, T. R. Zhang and Y. D. Yin, *J. Am. Chem. Soc.*, 2007, **129**, 8974–8975.
18 C. Goubault, F. Leal-Calderon, J. L. Viovy and J. Bibette, *Langmuir*, 2005, **21**, 3725–3729.
19 J. Rybczynski, U. Ebels and M. Giersig, *Colloid Surf. A-Physicochem. Eng. Asp.*, 2003, **219**, 1–6.
20 M. Golosovsky, Y. Saado and D. Davidov, *Appl. Phys. Lett.*, 1999, **75**, 4168–4170.
21 B. A. Grzybowski, X. Y. Jiang, H. A. Stone and G. M. Whitesides, *Phys. Rev. E*, 2001, **64**, 011603.
22 L. E. Helseth, *Langmuir*, 2005, **21**, 7276–7279.
23 E. Kun, W. J. Wen, K. F. Pal and K. N. Tu, *Phys. Rev. E*, 2001, **64**, 061503.
24 L. E. Helseth, R. M. Muruganathan, Y. Zhang and T. M. Fischer, *Langmuir*, 2005, **21**, 7271–7275.
25 E. M. Furst and A. P. Gast, *Phys. Rev. E*, 2000, **62**, 6916–6925.
26 C. J. Campbell and B. A. Grzybowski, *Philos. Trans. R. Soc. Lond. Ser. A-Math. Phys. Eng. Sci.*, 2004, **362**, 1069–1086.
27 S. L. Biswal and A. P. Gast, *Anal. Chem.*, 2004, **76**, 6448–6455.
28 J. P. Ge, Y. X. Hu, M. Biasini, W. P. Beyermann and Y. D. Yin, *Angew. Chem.-Int. Edit.*, 2007, **46**, 4342–4345.
29 J. P. Ge, T. Huynh, Y. P. Hu and Y. D. Yin, *Nano Lett.*, 2008, **8**, 931–934.
30 H. Singh, P. E. Laibinis and T. A. Hatton, *Nano Lett.*, 2005, **5**, 2149–2154.
31 B. A. Evans, A. R. Shields, R. L. Carroll, S. Washburn, M. R. Falvo and R. Superfine, *Nano Lett.*, 2007, **7**, 1428–1434.
32 C. Ooi, R. M. Erb and B. B. Yellen, *J. Appl. Phys.*, 2008, **103**, 07E910.
33 D. L. Hartsock, R. F. Novak and G. J. Chaundy, *J. Rheol.*, 1991, **35**, 1305–1326.
34 J. M. Vance and D. Ying, *J. Eng. Gas. Turbines Power-Trans. ASME*, 2000, **122**, 337–344.
35 B. F. Spencer, S. J. Dyke, M. K. Sain and J. D. Carlson, *J. Eng. Mech.-ASCE*, 1997, **123**, 230–238.
36 E. M. Furst and A. P. Gast, *Phys. Rev. E*, 2000, **61**, 6732–6739.
37 Z. Y. Wang, Z. Peng, K. Q. Lu and W. J. Wen, *Appl. Phys. Lett.*, 2003, **82**, 1796–1798.
38 T. B. Jones, R. D. Miller, K. S. Robinson and W. Y. Fowlkes, *J. Electrost.*, 1989, **22**, 231–244.
39 C. Tan and T. B. Jones, *J. Appl. Phys.*, 1993, **73**, 3593–3598.
40 T. B. Jones, *Electromechanics of particles*, Cambridge University Press, New York, 1995.
41 B. G. Prevo and O. D. Velev, *Langmuir*, 2004, **20**, 2099–2107.
42 K. Karunakar, M. Ranjan and K. S. Prabhu, *IEEE Trans. Magn.*, 1981, **17**, 2488–2492.
43 S. Gangwal, O. J. Cayre and O. D. Velev, *Langmuir*, 2008, **24**, 13312–13320.
44 S. O. Lumsdon, E. W. Kaler and O. D. Velev, *Langmuir*, 2004, **20**, 2108–2116.
45 S. O. Lumsdon, E. W. Kaler, J. P. Williams and O. D. Velev, *Appl. Phys. Lett.*, 2003, **82**, 949–951.
46 R. C. O'Handley, *Modern magnetic materials: principles and applications*, Wiley, New York, 2000.
47 K. Závěta, *Czech. J. Phys.*, 1956, **6**, 473–480.
48 D. Halliday, R. Resnick and J. Walker, *Fundamentals of physics: extended with Modern Physics*, Wiley, New York, 1997.
49 A. S. Arrott and R. Hertel, *IEEE Trans. Magn.*, 2007, **43**, 2911–2913.
50 A. S. Arrott and R. Hertel, *J. Appl. Phys.*, 2008, **103**, 07E739.
51 Y. L. Raikher and V. I. Stepanov, *J. Phys.-Condes. Matter*, 2008, **20**, 204120.

 This journal is © The Royal Society of Chemistry 2009